ICASSP 2024 - 2024 IEEE International Conference on Acoustics, Speech and Signal Processing (ICASSP) | 979-8-3503-4485-1/24/$31.00 ©2024 IEEE | DOI: 10.1109/ICASSP48485.2024.10448445

ENHANCED LOW-RANK AND SPARSE TUCKER DECOMPOSITION FOR IMAGE COMPLETION

Wenwu Gong, Zhejun Huang, Lili Yang *

Southern University of Science and Technology
Department of Statistics and Data Science
Shenzhen, 518055, China.

ABSTRACT

Recent advancements in low-rank tensor measures have addressed tensor completion challenges, particularly in image completion (IC) tasks. However, the most current low rankness is often based on the unfolding matrix's rank summation. Moreover, it ignores the local similarity or adapts oversmoothed regularization to the image data, which could be unreliable in high-level corruption recovery. This paper proposes a novel Tucker-based model to consider global and local information in imaging. Specifically, the weighted factor matrix rank and core tensor sparsity are used to encode the global low rankness, while graph regularization is employed to characterize the local similarity. This paper proposes a linearized alternating direction method (LADM) with easy subproblems for solving the IC task. Extensive experiments demonstrate the accuracy of our proposal, even under extreme cases, such as 99% missing scenario.

Index Terms— Enhanced Tucker decomposition, graph regularization, linearized alternating direction method, image completion

1. INTRODUCTION

Image completion (IC), a fundamental problem in computer vision, aims to recover the original image from its corrupted observation [1]. From the mathematics standpoint, recovering the lost information is a typical ill-posed inverse problem. Recently, low-rank tensor completion (LRTC) methods have been successfully applied to IC tasks [2, 3], where the tensor structure delivers intrinsic multidimensional information underlying image data. From the perspective of Bayesian, the LRTC problem can generally be expressed as a maximum a posterior (MAP) model:

$$\underset{\mathcal{X}}{\text{minimize}}\ L(\hat{\mathcal{X}}, \mathcal{T}) + \lambda R(\mathcal{X}), \tag{1}$$

where $L(\cdot,\cdot)$ measures the error between output image $\hat{\mathcal{X}}$ and corrupted input image $\mathcal{T}$, and $R(\cdot)$ is the tensor measure. Thus, the core of the IC task is to utilize prior structures rationally [4], such as low-rankness (global correlations in tensor image) and smoothness (local similarity across various image channels).

The low rankness has the following two folds. On the one hand, tensor rank minimization, including multilinear [5] and tubal ranks [6], has been commonly analyzed in LRTC problems. However, these methods do not work well for highly corrupted images and cannot simultaneously encode local similarity in imaging. On the other hand, low-rank tensor decomposition (LRTD) models [7, 8] perform more robustness and precisely, enhancing the learning capabilities of the LRTC model. The challenge associated with LRTD lies in constructing an appropriate decomposition model that effectively represents the underlying low-rank structure.

In this paper, we aim to answer three major open questions. Firstly, considering that the Tucker rank relaxation is not unique, constructing a rational low rankness in the Tucker model is crucial. Secondly, local similarity should not be neglected for multidimensional imaging. From the perspective of subspace learning, characterizing the within-mode similarity is essential to get more precise IC results. Finally, the Tucker-based model is a nonconvex optimization problem, which needs an efficient implementation algorithm to find the stationary points.

This paper combines global and local priors for the IC task, and Fig 1 gives a visual display for our proposal. We recover an image under the assumption of 'low rankness' and consider the Tucker model's factor graph regularization constraints to characterize the image's underlying local similarity. The main contributions of this paper are summarized as follows.

1. Motivated by [9] and [10], we use the weighted factor matrix rank and core tensor sparsity to encode the global low Tucker rank. Furthermore, the factor matrix weight is self-adaptive, and a tradeoff parameter is determined to compromise the low-rank and sparsity role.
2. To get a more accurate recovery performance, we con-

*Thanks to Shenzhen Science and Technology Plan platform and carrier special (Grant No. ZDSYS20210623092007023), Shenzhen Scientific Research Funding (Grant No. K22627501), and Guangdong Province Universities and Colleges Key Areas of Special Projects (Grant No. 2021222012) for funding.

sider graph regularization as an effective constraint to characterize the local similarity of imaging. We call our proposed model Enhanced Low-rank and Sparse Tucker Decomposition (E-LRSTD), which encodes global and local similarity of imaging simultaneously.

3. We minimize the proposed E-LRSTD model using the linearized alternating direction method (LADM) algorithm and reformulate it as the nuclear norm minimization and sparse coding problem, which deduces the closed-form updating rules.

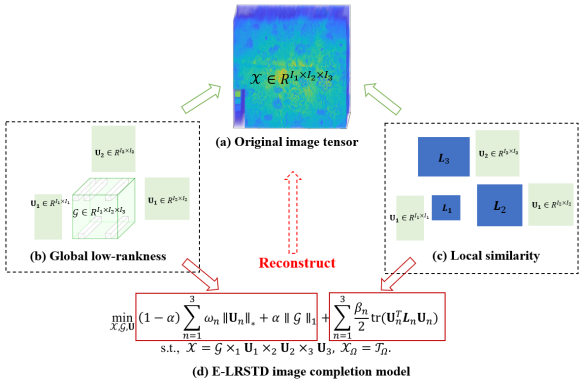

Fig. 1. Visual display for the proposed E-LRSTD model.

2. NOTATIONS AND RELATED WORKS

2.1. Notations

We give related concepts of Tucker decomposition as follows and present all notations used in this paper in Tab. 1.

Table 1. Notations

$\mathcal{X}, \mathbf{U}, \alpha$	A tensor, matrix and real value, respectively.
$\Omega, \bar{\Omega}$	Observed index set and its complement.
$\mathcal{S}_\eta(x)$	Shrinkage operator with η in component-wise.
$\mathcal{D}_\eta(\mathbf{U})$	SVD shrinkage of matrix $\mathbf{U}$.
$\mathcal{X}_\Omega$	Observed entries on the observed index.
$\times_n, \otimes$	Mode-n and Kronecker product.
tr	Trace operator.
$\|\cdot\|_F, \|\cdot\|_*$	Frobenius and nuclear norm.
$\mathbf{X}_{(n)}$	Mode-n unfolding of tensor $\mathcal{X}$.

Given a tensor $\mathcal{X} \in \mathbb{R}^{I_1 \times I_2 \times \cdots \times I_N}$, Tucker decomposition represented by a core tensor $\mathcal{G} \in \mathbb{R}^{I_1 \times I_2 \times \cdots \times I_N}$ multiplying matrix $\mathbf{U}_n \in \mathbb{R}^{I_n \times I_n}$ along each mode, i.e., $\mathcal{X} = \mathcal{G} \times_1 \mathbf{U}_1 \cdots \times_N \mathbf{U}_N = \mathcal{G} \times_{n=1}^{N} \mathbf{U}_n$. Based on the matrix Kronecker product $\otimes$, the Tucker decomposition can be written in the matrix form: $\mathbf{X}_{(n)} = \mathbf{U}_n \mathbf{G}_{(n)} \mathbf{V}_n^{\mathrm{T}}$, $\mathbf{V}_n = (\mathbf{U}_N \otimes \cdots \mathbf{U}_{n+1} \otimes \mathbf{U}_{n-1} \otimes \cdots \mathbf{U}_1)$ and the superscript 'T' represent matrix transpose.

Table 2. Some existing Tucker-based methods utilizing different priors

IC methods	Types of the priors		
	Low-rankness	Sparsity	Smoothness
E-LRSTD	✓	✓	✓
ARTD [4]		✓	✓
Transform-based [14]	✓	✓	
SBCD [10]	✓	✓	✓
logTucker [12]	✓		
ESP-LRTC [9]	✓		✓
KBR [8]	✓	✓	
STDC [17]	✓		✓

2.2. Related works

Low rankness measures are commonly used prior structures in the LRTC problem. For example, matricization terms, such as rank-summation [5, 11] and its nonconvex relaxation [12], were proposed for the IC task. The tensor trains (TT) [13] formulation, an extension of Tucker, also performed well in the LRTC problem. Furthermore, the sparsity measure defined by rank-1 Kronecker bases and nonzero-block core tensor [8] is first proposed to encode the low rankness in image recovery. Also, exploiting the low-rank structure induced by the transformer [14, 15] was well-studied in the IC task.

To capture the local similarity, the smoothness constraints, such as total variation (TV) terms [16] and graph regularization [17], are proposed to enhance model performance for the IC task. Furthermore, some parameter-free tuning methods, such as hierarchical priors [18, 19], are proven workable under a fully Bayesian treatment.

The joint priors of low rankness and smoothness were also researched in various low-rank Tucker models [4, 9, 10]. These methods perform well for the IC task, especially the recent Tucker decomposition combining the graph regularization [4] and the low Tucker rank tensor completion method with given rank [10]. This work differs from our proposed E-LRSTD in that the low rankness is exploited using nuclear norm and sparsity in ARTD [4]. More importantly, a rational low-rank and sparsity Tucker model combined with local similarity has not been thoroughly studied. The main attributes of our proposed E-LRSTD model and that of several Tucker-based popular IC methods are listed in Tab. 2.

3. PROPOSED MODEL

We propose a Tucker-based model to consider global and local information for the IC task. To avoid the highly computational complexity of tensor unfolding and matrix decomposition in tensor nuclear norm minimization, we use the weighted factor matrix rank and core tensor sparsity to encode the global low Tucker rank. We consider graph regularization

as the smoothness constraint to characterize the local similarity of the image data, which further enhances the model performance. Furthermore, an LADM-based optimization algorithm is designed to solve the proposed model.

3.1. Enhanced LRSTD

We focus on low rank and sparsity priors to Tucker decomposition and define the LRSTD model for the IC task as (2)

$$\begin{aligned} \min_{\mathcal{G},\mathbf{U},\mathcal{X}} \ & (1-\alpha)\sum_{n=1}^{N} w_n \left\|\mathbf{U}_n\right\|_* + \alpha\|\mathcal{G}\|_1 \\ \text{s.t.,} \ & \mathcal{X} = \mathcal{G} \times_{n=1}^{N} \mathbf{U}_n, \ \mathcal{X}_\Omega = \mathcal{T}_\Omega. \end{aligned} \tag{2}$$

Motivated by the local similarity in the image data, we further introduce the proposed E-LRSTD model as (3)

$$\begin{aligned} \min_{\mathcal{G},\mathbf{U},\mathcal{X}} \ & \lambda\sum_{n=1}^{N} \omega_n \left\|\mathbf{U}_n\right\|_* + \|\mathcal{G}\|_1 + \sum_{n=1}^{N} \tfrac{\beta_n}{2} \operatorname{tr}\left(\mathbf{U}_n^{\mathrm{T}}\mathbf{L}_n\mathbf{U}_n\right) \\ \text{s.t.,} \ & \mathcal{X} = \mathcal{G} \times_1 \mathbf{U}_1 \cdots \times_N \mathbf{U}_N, \ \mathcal{X}_\Omega = \mathcal{T}_\Omega, \\ & \lambda = \tfrac{1-\alpha}{\alpha}, \ 0 < \alpha \leq 1 \end{aligned} \tag{3}$$

where the Laplace matrix $\mathbf{L}_n$ captures the underlying multimodal correlations in the image data. If $\alpha = 1$, the E-LRSTD model degrades into an ARTD model.

***Remark*: Minimizing the factor matrix nuclear norm in Tucker decomposition is equivalence to minimizing the unfolding matrix nuclear norm [10]. The Laplacian-based matrix can be constructed using prior information about the image. Besides, graph regularization is a kind of subspace learning that helps to reveal local similarities [4].**

3.2. Optimization

We define the augmented Lagrange function $\mathbf{L}_\mu(\dots)$ (4) to solve model (3)

$$\begin{aligned} & \lambda\sum_{n=1}^{N} \omega_n \left\|\mathbf{U}_n\right\|_* + \|\mathcal{G}\|_1 + \sum_{n=1}^{N} \tfrac{\beta_n}{2} \operatorname{tr}\left(\mathbf{U}_n^{\mathrm{T}}\mathbf{L}_n\mathbf{U}_n\right) \\ & + \tfrac{\mu}{2}\left\|\mathcal{X} - \mathcal{G} \times_{n=1}^{N} \mathbf{U}_n\right\|_{\mathrm{F}}^2 + \left\langle \mathcal{Y}, \mathcal{X}_\Omega - \mathcal{G} \times_{n=1}^{N} \mathbf{U}_n \right\rangle \end{aligned} \tag{4}$$

where μ is a positive scalar that adaptively changing, and $\mathcal{Y}$ is the Lagrange multiplier.

Optimization of $\mathcal{G}$. With other parameters fixed, we have

$$\begin{aligned} \hat{\mathcal{G}} &= \mathcal{S}_{\frac{1}{\mu L_{\mathcal{G}}}}(\tilde{\mathcal{G}} - \frac{1}{L_{\mathcal{G}}}\nabla_{\mathcal{G}} f\left(\tilde{\mathcal{G}}\right)), \\ \nabla_{\mathcal{G}} f(\mathcal{G}) &= \mathcal{G} \times_{n=1}^{N} \mathbf{U}_n^{\mathrm{T}}\mathbf{U}_n - \left(\mathcal{X} + \frac{\mathcal{Y}}{\mu}\right) \times_{n=1}^{N} \mathbf{U}_n^{\mathrm{T}}. \end{aligned} \tag{5}$$

Optimization of $\mathbf{U}_n$. $\mathbf{U}_n$ is given by (6) with $\mathbf{U}_j, j \neq n$ and other parameters fixed ($w_n = \lambda\omega_n$).

$$\begin{aligned} \hat{\mathbf{U}}_n &= \mathcal{D}_{\frac{w_n}{L_{\mathbf{U}_n}}}\left(\tilde{\mathbf{U}}_n - \frac{1}{L_{\mathbf{U}_n}}\nabla_{\mathbf{U}_n} f\left(\tilde{\mathbf{U}}_n\right)\right). \\ \nabla_{\mathbf{U}_n} f(\mathbf{U}_n) &= \mu\mathbf{U}_n\mathbf{G}_{(n)}\mathbf{V}_n^{\mathrm{T}}\mathbf{V}_n\mathbf{G}_{(n)}^{\mathrm{T}} + \beta\mathbf{L}_n\mathbf{U}_n \\ &\quad - \left(\mu\mathbf{X}_{(n)} + \mathbf{Y}_{(n)}\right)\mathbf{V}_n\mathbf{G}_{(n)}^{\mathrm{T}}, \\ L_{\mathbf{U}_n} &= \left\|\mu\mathbf{G}_{(n)}\mathbf{V}_n^{\mathrm{T}}\mathbf{V}_n\mathbf{G}_{(n)}^{\mathrm{T}}\right\|_2 + \left\|\beta_n\mathbf{L}_n\right\|_2. \end{aligned} \tag{6}$$

***Remark*: In the LADM-based algorithm, we approximate the smooth function using extrapolated points $\tilde{\mathcal{G}}$ and $\tilde{\mathbf{U}}$. Under the Nesterov accelerated strategy, Algorithm 1 achieves the optimal $\mathcal{O}(1/k^2)$ convergence rate [20].**

Optimization of $\mathcal{X}$.

$$\hat{\mathcal{X}}_\Omega = \mathcal{T}_\Omega, \ \hat{\mathcal{X}}_{\bar{\Omega}} = \left(\hat{\mathcal{G}} \times_{n=1}^{N} \hat{\mathbf{U}}_n - \frac{\mathcal{Y}_k}{\mu_k}\right)_{\bar{\Omega}}. \tag{7}$$

Updating the multipliers $\mathcal{Y}$.

$$\begin{aligned} \mathcal{Y}^{k+1} &= \hat{\mathcal{Y}} + \mu^k\left(\hat{\mathcal{X}} - \hat{\mathcal{G}} \times_{n=1}^{N} \hat{\mathbf{U}}_n\right), \\ \mu^{k+1} &= \rho\mu^k, \ \rho \in [1.1, 1.2]. \end{aligned} \tag{8}$$

We conclude the LADM algorithm for the IC in Algorithm 1. A rigorously theoretical convergence of the LADM algorithm is difficult to obtain due to the nonconvexity and nonseparability of Tucker decomposition [17]. Here, we provide the numerical convergence of the proposed algorithm in Fig. 2.

Algorithm 1 LADM solver for E-LRSTD model

Input: Corrupted image $\mathcal{T}$, observed entries Ω.
Output: Recovered image $\hat{\mathcal{X}}$.
Initialize: $\mathcal{G}^0, \{\mathbf{U}_n^0\}$ $(1 \leq n \leq N)$, $0 < \alpha \leq 1$;
$\mathcal{X}_\Omega = \mathcal{T}_\Omega$, $\mathcal{X}_{\bar{\Omega}} = \text{mean}(\mathcal{T}_{\bar{\Omega}})$;
while $k < K$ **do**
  Optimize $\mathcal{G}^{k+1}$ via (5) with other variables fixed;
  Optimize all $\mathbf{U}_n^{k+1}$ via (6) with other variables fixed;
  Optimize $\mathcal{X}^{k+1}$ via (7) with other variables fixed;
  Update multipliers $\mathcal{Y}$ using (8)
  Update $\tilde{\mathcal{G}}^{k+1}$ and $\tilde{\mathbf{U}}_n^{k+1}$ using acceleration strategy;
  until $\left\|\mathcal{X}^{k+1} - \mathcal{X}^k\right\|_F \left\|\mathcal{X}^k\right\|_F^{-1} <$ tol are satisfied.
end while
return $\hat{\mathcal{X}} = \mathcal{X}^{K+1}$.

4. NUMERICAL EXPERIMENTS

We present the experimental results on real image datasets to demonstrate the efficiency of the proposed E-LRSTD model. The code is released at `https://github.com/GongWenwuu/ELRSTD`.

Datasets: The color image USC-SIPI [1] and the multispectral image from CAVE [2] database are both resized to 256 × 256 for all spectral bands. The quality of recovery results is measured by the peak signal-to-noise ratio (PSNR) and the structural similarity index (SSIM), where higher PSNR and SSIM values indicate better results.

Implementation details: We randomly sample 10% of images and initial the Tucker decomposition randomly. The low rankness parameter is chosen as 0.5 for all images. We

[1] `https://sipi.usc.edu/database/database.php`
[2] `https://www.cs.columbia.edu/CAVE/databases/multispectral/`

then calculate the factor matrix SVD values to deliver $\{\omega_n\}$, which is data-driven. Fig. 2 (left) shows the Root Mean Square Error (RMSE) curves versus the iteration number of the Algorithm 1. It can be seen that the RMSE keeps decreasing as the iteration number increases, and the values stabilize after only about 300 iterations, which implies the proposed algorithm's numerical convergence. We also discuss the efficiency of the proposed method with and without Nesterov acceleration in Fig 2 (right). Results show that the Nesterov strategy performs better and speeds up its convergence, especially for the multispectral image Cloth.

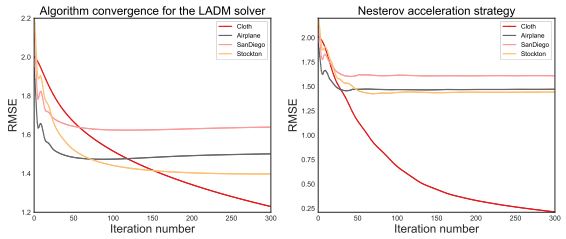

Fig. 2. Convergence results using Algorithm 1.

Ablation study: We first discuss the effect of the low rankness compared with Tucker-based SBCD [10], tubal-based [6], TT-based [13], and matrices-based []. Fig. 3 (left) shows that LRSTD performs better when sample ratios (SRs) are lower than 20%. Guided by [4], we determine the parameter $\{\beta_n\}$ using different mode-n unfolding matrices given the image tensor. We denote 'LRSTD1' (only mode-3 constraint) to discuss the effect of the graph regularization in terms of PSNR. The results are shown in Fig. 3 (right), which implies that the proposed graph regularization is essential for our IC task.

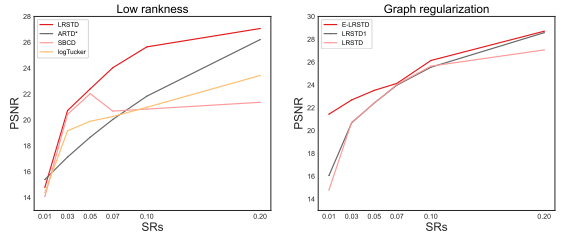

Fig. 3. PSNR versus SRs for low rankness and regularization.

Model comparison: We select baseline models, including TMac [11], tSVD [6], BCPF [18], TT [13], KBR [8] and ESP-LRTC [9] to compare the numeric results. Our experiments consider six random missing scenarios: 1%, 3%, 5%, 7%, 10%, and 20%. Fig. 4 and Fig 5 show the comparison results regarding PSNR and SSIM. It can be seen that E-LRSTD achieves the best values for all images, further validating the proposed method's robustness over all spectral bands. On the PSNR index, E-LRSTD achieves 0.8 dB improvement for RGB images and 0.4 dB improvement for Cloth on average.

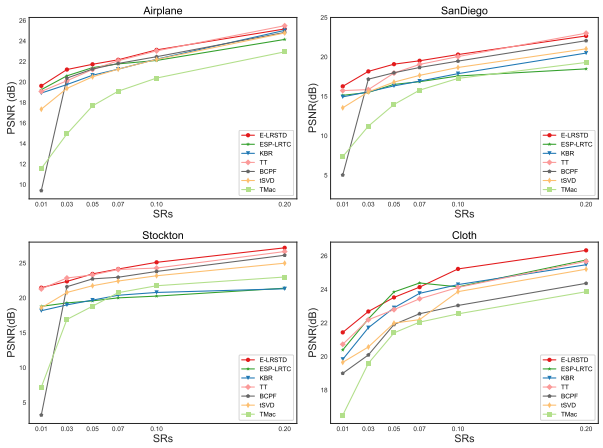

Fig. 4. Comparison results of PSNR scores concerning SRs.

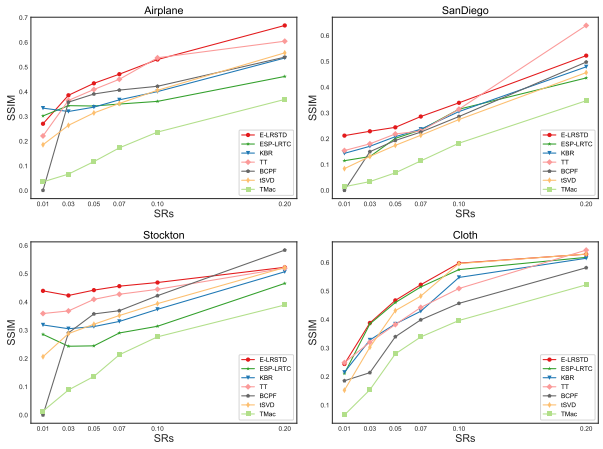

Fig. 5. Comparison results of SSIM values concerning SRs.

5. CONCLUSION

This paper introduces a Tucker-based model combined with global and local information (E-LRSTD) to address the IC task. It is demonstrated that the global and local priors are important in tensor completion. We design an efficient solver LADM and deduce the closed-form updating rules. Extensive experiments on real-world images show that E-LRSTD outperforms the others, especially when the missing ratios are high, i.e. $SR \leq 0.1$. For the high computational cost of large-scale tensors, one can consider the fast Fourier transform to address this issue [21].

6. REFERENCES

[1] Lei Zhang and Wangmeng Zuo, "Image restoration: From sparse and low-rank priors to deep priors [lecture notes]," *IEEE Signal Process Mag*, vol. 34, no. 5, pp. 172–179, 2017.

[2] Xile Zhao, Jinghua Yang, Tianhui Ma, Taixiang Jiang, Michael K. Ng, and Tingzhu Huang, "Tensor completion via complementary global, local, and nonlocal priors," *IEEE Trans. Image Process.*, vol. 31, pp. 984–999, 2022.

[3] Hailin Wang, Jiangjun Peng, Wenjin Qin, Jianjun Wang, and Deyu Meng, "Guaranteed tensor recovery fused low-rankness and smoothness," *IEEE Trans. Pattern Anal. Mach. Intell.*, vol. 45, no. 9, pp. 10990–11007, 2023.

[4] Wenwu Gong, Zhejun Huang, and Lili Yang, "Accurate regularized tucker decomposition for image restoration," *Appl. Math. Model.*, vol. 123, no. 11, pp. 75–86, 2023.

[5] Ji Liu, Przemyslaw Musialski, Peter Wonka, and Jieping Ye, "Tensor completion for estimating missing values in visual data," *IEEE Trans. Pattern Anal. Mach. Intell.*, vol. 35, no. 1, pp. 208–220, 2013.

[6] Zemin Zhang and Shuchin Aeron, "Exact tensor completion using t-svd," *IEEE Trans. Signal Process.*, vol. 65, no. 6, pp. 1511–1526, 2017.

[7] Qibin Zhao, Liqing Zhang, and Andrzej Cichocki, "Bayesian CP factorization of incomplete tensors with automatic rank determination," *IEEE Trans. Pattern Anal. Mach. Intell.*, vol. 37, no. 9, pp. 1751–1763, 2015.

[8] Qi Xie, Qian Zhao, Deyu Meng, and Zongben Xu, "Kronecker-basis-representation based tensor sparsity and its applications to tensor recovery," *IEEE Trans. Pattern Anal. Mach. Intell.*, vol. 40, no. 8, pp. 1888–1902, 2018.

[9] Jize Xue, Yongqiang Zhao, Wenzhi Liao, Jonathan Cheung-Wai Chan, and Seong G. Kong, "Enhanced sparsity prior model for low-rank tensor completion," *IEEE Trans. Neural Networks Learn. Syst.*, vol. 31, no. 11, pp. 4567–4581, 2020.

[10] Quan Yu, Xinzhen Zhang, Yannan Chen, and Liqun Qi, "Low Tucker rank tensor completion using a symmetric block coordinate descent method," *Numer Linear Algebra Appl*, vol. 30, no. 3, pp. e2464, 2023.

[11] Yangyang Xu, Ruru Hao, Wotao Yin, and Zhixun Su, "Parallel matrix factorization for low-rank tensor completion," *Inverse Probl Imaging*, vol. 9, no. 2, pp. 601–624, 2015.

[12] Chengfei Shi, Zhengdong Huang, Li Wan, and Tifan Xiong, "Low-rank tensor completion based on non-convex logdet function and tucker decomposition," *Signal Image Video Process*, vol. 15, no. 02, pp. 1169–1177, 2021.

[13] Johann A. Bengua, Ho N. Phien, Hoang Duong Tuan, and Minh N. Do, "Efficient tensor completion for color image and video recovery: Low-rank tensor train," *IEEE Trans. Image Process.*, vol. 26, no. 5, pp. 2466–2479, 2017.

[14] Chenjian Pan, Chen Ling, Hongjin He, Liqun Qi, and Yanwei Xu, "Sparse + low-rank tensor completion approach for recovering images and videos," 2022.

[15] Benzheng Li, Xile Zhao, Tengyu Ji, Xiongjun Zhang, and Tingzhu Huang, "Nonlinear transform induced tensor nuclear norm for tensor completion," *J Sci Comput*, vol. 92, no. 83, 2022.

[16] Xutao Li, Yunming Ye, and Xiaofei Xu, "Low-rank tensor completion with total variation for visual data inpainting," in *Proceedings of the AAAI Conference on Artificial Intelligence (AAAI)*, 2017, pp. 2210–2216.

[17] Yilei Chen, Chiou-Ting Hsu, and Hong-Yuan Mark Liao, "Simultaneous tensor decomposition and completion using factor priors," *IEEE Trans. Pattern Anal. Mach. Intell.*, vol. 36, no. 3, pp. 577–591, 2014.

[18] Qibin Zhao, Liqing Zhang, and Andrzej Cichocki, "Bayesian cp factorization of incomplete tensors with automatic rank determination," *IEEE Trans. Pattern Anal. Mach. Intell.*, vol. 37, no. 9, pp. 1751–1763, 2015.

[19] Jize Xue, Yongqiang Zhao, Yuanyang Bu, Jonathan Cheung-Wai Chan, and Seong G. Kong, "When laplacian scale mixture meets three-layer transform: A parametric tensor sparsity for tensor completion," *IEEE Trans Cybern*, vol. 52, no. 12, pp. 13887–13901, 2022.

[20] Junfeng Yang and Xiaoming Yuan, "Linearized augmented lagrangian and alternating direction methods for nuclear norm minimization," *Math. Comput.*, vol. 82, pp. 301–329, 2012.

[21] Ryuki Yamamoto, Hidekata Hontani, Akira Imakura, and Tatsuya Yokota, "Fast algorithm for low-rank tensor completion in delay-embedded space," in *2022 IEEE/CVF Conference on Computer Vision and Pattern Recognition (CVPR)*, 2022, pp. 2048–2056.